

Weak localisation in magnetoresistance and valley symmetry in graphene

E. M. McCann¹, K. Kchedzhi¹, V. Ladimir I. Fal'ko¹, H. Suzuura², T. Ando³, and B. L. A. Ithuler⁴¹Department of Physics, Lancaster University, Lancaster, LA1 4YB, UK²Division of Applied Physics, Graduate School of Engineering, Hokkaido University, Sapporo 060-8628, Japan³Department of Physics, Tokyo Institute of Technology,

2-12-1 Ookayama, Meguro-ku, Tokyo 152-8551, Japan

⁴Physics Department, Columbia University, 538 West 120th Street, New York, NY 10027

Due to the chiral nature of electrons in a monolayer of graphite (graphene) one can expect weak antiblocalisation and a positive weak-field magnetoresistance in it. However, trigonal warping (which breaks $p\pi$ symmetry of the Fermi line in each valley) suppresses antiblocalisation, while intervalley scattering due to atomically sharp scatterers in a realistic graphene sheet or by edges in a narrow wire tends to restore conventional negative magnetoresistance. We show this by evaluating the dependence of the magnetoresistance of graphene on relaxation rates associated with various possible ways of breaking a 'hidden' valley symmetry of the system.

PACS numbers: 73.63.Bd, 71.70.Dj, 73.43.Cd, 81.05.Jw

The chiral nature [1, 2, 3, 4, 5] of quasiparticles in graphene (monolayer of graphite), which originates from its honeycomb lattice structure and is revealed in quantum Hall effect measurements [6, 7], is attracting a lot of interest. In recently developed graphene-based transistors [6, 7] the electronic Fermi line consists of two tiny circles [8] surrounding corners K of the hexagonal Brillouin zone [9], and quasiparticles are described by 4-component Bloch functions $\psi = [\psi_{K+;A}, \psi_{K+;B}, \psi_{K-;A}, \psi_{K-;B}]$, which characterise electronic amplitudes on two crystalline sublattices (A and B), and the Hamiltonian

$$\hat{H} = v_z \mathbf{p} \cdot [\mathbf{p}_x^2 - \mathbf{p}_y^2] - 2v_y p_x p_y; \quad (1)$$

Here, we use direct products of Pauli matrices $\sigma_{x,y,z}$ acting in the sublattice space (A; B) and $\hat{\sigma}_{x,y,z}$ acting in the valley space (K) to highlight the form of \hat{H} in the non-equivalent valleys [9]. Near the center of each valley electron dispersion is determined by the Dirac-type part $v\mathbf{p}$ of \hat{H} . It is isotropic and linear. For the valley K+, the electronic excitations with momentum \mathbf{p} have energy $v\mathbf{p}$ and are chiral with $\mathbf{p} \cdot \hat{\mathbf{p}} = 1$, while for holes the energy is $-v\mathbf{p}$ and $\mathbf{p} \cdot \hat{\mathbf{p}} = -1$. In the valley K-, the chirality is inverted: it is $\mathbf{p} \cdot \hat{\mathbf{p}} = -1$ for electrons and $\mathbf{p} \cdot \hat{\mathbf{p}} = 1$ for holes. The quadratic term in Eq. (1) violates the isotropy of the Dirac spectrum and causes a weak trigonal warping [9].

Due to the chirality of electrons in a graphene-based transistor, charges trapped in the substrate or on its surface cannot scatter carriers in exactly the backwards direction [3, 8], provided that the trap is remote from the graphene sheet by more than the lattice constant. In the theory of quantum transport [10] the suppression of backscattering is associated with weak anti-localisation (WAL) [11]. For purely potential scattering, possible WAL in graphene has recently been related to the Berry phase specific to the Dirac fermions, though it has also been noticed that conventional weak localisation (WL) may be restored by intervalley scattering [12, 13].

In this Letter we show that the WL magnetoresistance

in graphene directly reflects the degree of valley symmetry breaking by the warping term in the free-electron Hamiltonian (1) and by atomically sharp disorder. To describe the valley symmetry, we introduce two sets of 4x4 Hermitian matrices: 'isospin' $\tilde{\sigma} = (\sigma_x, \sigma_y, \sigma_z)$ and 'pseudospin' $\tilde{\sigma} = (\hat{\sigma}_x, \hat{\sigma}_y, \hat{\sigma}_z)$. These are defined as

$$\tilde{\sigma}_x = \sigma_z \quad \tilde{\sigma}_y = \sigma_z \quad \tilde{\sigma}_z = 0 \quad \tilde{\sigma}_i = (2) \quad (2)$$

$$\tilde{\sigma}_x = \sigma_x \quad \tilde{\sigma}_y = \sigma_y \quad \tilde{\sigma}_z = \sigma_z \quad \tilde{\sigma}_i = 0; \quad (3)$$

and form two mutually independent algebras, $[\tilde{\sigma}_i, \tilde{\sigma}_j] = 0$,

$$[\tilde{\sigma}_1, \tilde{\sigma}_2] = 2i\tilde{\sigma}_3 \quad \tilde{\sigma}_i [\tilde{\sigma}_1, \tilde{\sigma}_2] = 2i\tilde{\sigma}_1 \quad (4)$$

which determine two commuting subgroups of the group U_4 of unitary transformations [14] of a 4-component : an isospin (sublattice) group SU_2 $\text{fe}^{i\pi/2}$ and a pseudospin (valley) group SU_2 $\text{fe}^{i\pi/2}$.

The operators $\tilde{\sigma}$ and $\tilde{\sigma}$ help us to represent the electron Hamiltonian in weakly disordered graphene as

$$\hat{H} = v\tilde{\sigma}_z \mathbf{p} + \hat{h}_w + \hat{h}_u(\mathbf{r}) + \sum_{s=1}^4 u_{s;1}(\mathbf{r}); \quad (4)$$

$$\text{where } \hat{h}_w = \tilde{\sigma}_x (\tilde{\sigma}_y \mathbf{p}_z - \tilde{\sigma}_z \mathbf{p}_y) \tilde{\sigma}_x:$$

The Dirac-type part $v\tilde{\sigma}_z \mathbf{p}$ of \hat{H} in Eq.(4) and potential disorder $\hat{h}_u(\mathbf{r})$ [it is a 4x4 unit matrix and $h_u(\mathbf{r}) = u^2(\mathbf{r} - \mathbf{r}')$] do not contain pseudospin operators $\tilde{\sigma}_i$, thus, they remain invariant with respect to the transformations from the group SU_2 . Note that $\tilde{\sigma}$ and $\tilde{\sigma}$ change sign under the inversion of time [9], so that products $u_{s;1}$ are t ! t invariant and (together with the unit matrix $\hat{1}$) can be used as a basis to represent non-magnetic static disorder. Below, we assume that disorder due to remote charges dominates the elastic scattering rate, $u^2 = \rho_F = (2\pi^2 v)^2$ is the density of states of quasiparticles per spin in one valley. All other types of disorder which originate from atomically sharp defects [15, 16] and break the SU_2 pseudospin

symmetry of the system are included in a random matrix $u_{s,z}(r)$. In particular, $u_{z,z}(r)$ describes different on-site energies on the A and B sublattices, $u_{x,z}(r)$ and $u_{y,z}(r)$ play the role of a valley-antisymmetric vector potential due to disorder in A-B hopping elements, and $u_{s,x}(r)$ and $u_{s,y}(r)$ take into account inter-valley scattering. Also, the warping term, \hat{h}_w , lifts SU_2 -symmetry, though it remains invariant under pseudospin rotations around the z-axis.

Due to hidden SU_2 symmetry of the dominant part of the free-electron Hamiltonian and disorder in Eq. (4), pseudospin can be used as a quantum number to classify the two-particle correlation functions, 'Cooperons' which determine the form of the interference correction to the conductivity, g . Below, we show that the latter is determined by the interplay of one pseudospin singlet (C^0) and three triplet ($C^{x,y,z}$) Cooperons, $g = C^0 + C^z + C^x + C^y$, some of which are suppressed due to a lower symmetry of the Hamiltonian in realgraphene structures. That is, the 'warping' term \hat{h}_w and the disorder $u_{s,z}$ suppress intravalley Cooperons $C^{x,y}$ and wash out the Berry phase effect and WYL, whereas intervalley disorder $u_{x(y)}u_{s,x(y)}(r)$ suppresses C^z and restores weak localisation [10] of electrons, provided that their phase coherence lasts long enough. This results in a WYL-type negative weak field magnetoresistance in graphene which is strongly suppressed (down to zero) in samples with a longer intervalley scattering time, as we describe in detail at the end of this Letter.

To describe quantum transport of 2D electrons in graphene we (a) evaluate the disorder-averaged one-particle Green functions, vertex corrections, Drude conductivity and transport time; (b) classify Cooperon modes and derive equations for those which are gapless in the limit of purely potential disorder; (c) analyse 'Hikami boxes' [10, 11] for the weak localisation diagram paying attention to a peculiar form of the current operator for Dirac electrons and evaluate the interference correction to conductivity leading to the WYL magnetoresistance. In these calculations, we treat trigonal warping \hat{h}_w in the free-electron Hamiltonian Eqs. (1,4) perturbatively, assume that potential disorder $\hat{u}(r)$ dominates in the elastic scattering rate, $1_0 = u^2 \sim$, and take into account all other types of disorder when we determine the relaxation spectra of low-gap Cooperons.

(a). Using the standard methods of the diagrammatic technique for disordered systems [10, 11] and assuming that $p_F v \sim$, we obtain the disorder averaged single-particle Green's function,

$$\hat{G}^{R=A}(p; \tau) = \frac{\frac{R=A}{2} + v \sim p}{v^2 p^2}; \quad R=A = \frac{1}{2} i \sim_0^{-1}:$$

Note that, for the Dirac-type particles described in Eq. (1), the current operator is a momentum-independent matrix vector, $\hat{v} = v \sim$. As a result, the current vertex v_j ($j = x, y$), which appears as a block in Fig. 1(a)

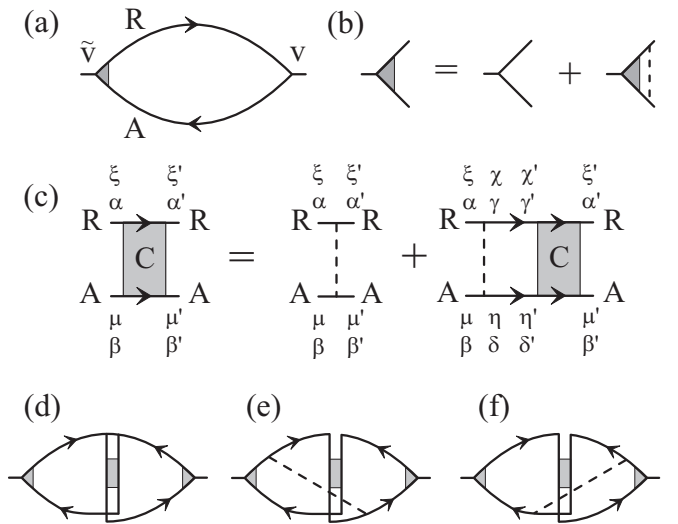


FIG. 1: (a) Diagram for the Drude conductivity with (b) the vertex correction. (c) Bethe-Salpeter equation for the Cooperon propagator with valley indices and AB lattice indices. (d) Bare 'Hikami box' relating the conductivity correction to the Cooperon propagator with (e) and (f) dressed 'Hikami boxes'. Solid lines represent disorder-averaged $G^{R=A}$, dashed lines represent disorder.

describing the Drude conductivity,

$$g_{jj} = \frac{e^2}{\sim} \frac{Z}{(2\pi)^2} \text{Tr} \frac{n}{v_j \hat{G}^R(p; \tau) \hat{v}_j \hat{G}^A(p; \tau)}; \\ = 4e^2 D; \text{ with } D = v^2_0 - \frac{1}{2} v^2 \text{tr}; \quad (5)$$

is renormalised by vertex corrections [15] in Fig. 1(b): $v = 2\tilde{v} = 2v \sim$. Here 'Tr' stands for the trace over the AB and valley indices. Using the Einstein relation in Eq. (5), we see that due to the anisotropy of scattering [i.e., lack of backscattering from an individual potential scatterer due to the electron chirality and the isospin conservation by $\hat{u}(r)$] the transport time in graphene is twice the scattering time, $\text{tr} = 2_0$. Note that in Eq.(5) spin degeneracy has been taken into account.

(b). The WYL correction to the conductivity is associated with the disorder-averaged two-particle correlation function $C^{x,y,z}$ known as the Cooperon. It obeys the Bethe-Salpeter equation represented diagrammatically in Fig. 1(c). The shaded blocks in Fig. 1(c) are infinite series of ladder diagrams, while the dashed lines represent the correlator of the disorder in Eq. (4). Here, the valley indices (K) of the Dirac-type electron are included as superscripts with incoming 0 and outgoing 0 , and the sublattice (AB) indices as subscripts 0 and 0 .

Using an analogy with real electron spin, we classify Cooperons in graphene as iso- and pseudospin singlets

and triplets,

$$C_{s_1 s_2}^{l_1 l_2} = \frac{1}{4} \begin{matrix} & X & X \\ & ; & ; & ; & ; & ; & ; & ; \\ & ; & ; & 0 & 0 & & & \\ & & & ; & ; & 0 & 0 & \\ & & & & & s_2 & y & l_2 & y \\ & & & & & 0 & 0 & & 0 & 0 \end{matrix} : \quad (6)$$

Such a classification of modes is permitted by the commutation of the iso- and pseudospin operators \sim and \sim in Eqs. (2,3,6), $[s; l] = 0$. To select the isospin singlet ($s = 0$) and triplet ($s = x; y; z$) Cooperon components (scalar and vector representation of the group SU_2 \rightarrow $fe^{i\pi} \sim g$), we project the incoming and outgoing Cooperon indices onto matrices y_{s_1} and $s_2 y$, respectively. The pseudospin singlet ($l = 0$) and triplet ($l = x; y; z$) Cooperons (scalar and vector representation of the 'valley' group SU_2 \rightarrow $fe^{i\pi} \sim g$) are determined by the projection of $C_{s_1 s_2}^{l_1 l_2}$ onto matrices $y_{l_1} (l_2 y)$ and are accounted for by superscript indices in $C_{s_1 s_2}^{l_1 l_2}$.

For 'diagonal' disorder $\hat{u}(r)$, the Bethe-Salpeter equation, Fig. 1(c) takes the form

$$C_{s_1 s_2}^{l_1 l_2}(q) = \begin{matrix} & 0 & l_1 l_2 & s_1 s_2 \\ & + & \frac{1}{4} & X \\ & & & 0 \sim s_1 \\ & & & n & h & i_t & o \\ & & & Tr & s & y & l & y & G_p^{R \sim} & + & y & l & y & s_1 G_{\sim q}^A & p & : \end{matrix}$$

It leads to a series of coupled equations for the Cooperon modes C_{ss}^{11} C_s^1 . It turns out that for potential disorder $\hat{u}(r)$ isospin-singlet modes C_0^1 are gapless in all (singlet and triplet) pseudospin channels, whereas triplet modes C_x^1 and C_y^1 have relaxation gaps $\frac{1}{x} = \frac{1}{y} = \frac{1}{2}$ and C_z^1 have gaps $\frac{1}{z} = \frac{1}{0}$. When obtaining the diffusion equations for the Cooperons using the gradient expansion of the Bethe-Salpeter equation we take into account its matrix structure. We find that isospin-singlets C_0^1 are coupled to the triplets C_x^1 and C_y^1 in linear order in the small wavevector q , so that the derivation of the diffusion operator for the isospin-singlet components would be incorrect if coupling to the gapful modes were neglected. The matrix equation for each set of four Cooperons ($C_0^1; C_x^1; C_y^1; C_z^1$) C^1 has the form

$$\begin{matrix} 0 & \frac{1}{2}v^2 & 0 & q^2 & + & 0 & i! & \frac{1}{2}vq_x & \frac{1}{2}vq_y & 0 & 1 \\ B & \frac{1}{2}vq_x & & & & \frac{1}{2} & 0 & 1 & 0 & 0 & C \\ C & \frac{1}{2}vq_y & & & & 0 & & \frac{1}{2} & 0 & 1 & A \\ 0 & 0 & & 0 & & 0 & & 0 & & 0 & 1 \end{matrix} : \quad C^1 = 1:$$

After the isospin-triplet modes were eliminated, the diffusion operator for each of the four gapless/low-gap modes C_0^1 becomes $D q^2 + i! + \frac{1}{0}$, where $D = \frac{1}{2}v^2$ $\text{tr} = v^2$.

Symmetry-breaking perturbations lead to relaxation gaps $\frac{1}{0}$ in the otherwise gapless pseudospin-triplet components, $C_0^x; C_0^y; C_0^z$ of the isospin-singlet Cooperon C_0^1 , though they do not generate a relaxation of the

pseudospin-singlet C_0^0 protected by the time-reversal symmetry of the Hamiltonian (4). We include all scattering mechanisms described in Eq. (4) in the corresponding disorder correlator (dashed line) on the r.h.s. of the Bethe-Salpeter equation and in the scattering rate in the disorder-averaged $G^{R=A}$, as $\hat{u}^1 = \hat{u}_0^1 + \hat{u}_{s1}^1 + \hat{u}_{s2}^1$. For simplicity, we assume that different types of disorder are uncorrelated, $u_{s1}(r)u_{s2}(r^0)i = u_{s1}^2 u_{s2}^0 \hat{u}(r^0)$ and, on average, isotropic in the $x-y$ plane: $u_{x1}^2 = u_{y1}^2$ $u_{x1}^2, u_{sx}^2 = u_{sy}^2 = u_s^2$. We parameterize them by scattering rates $\hat{u}_{s1}^1 = \hat{u}_{s2}^1 = \hat{u}_s^1$, where $u_{sx}^1 = u_{sy}^1 = u_s^1$ and $\hat{u}_{x1}^1 = \hat{u}_{y1}^1 = \hat{u}_z^1$ due to the $x-y$ plane isotropy of disorder, which are combined into the intervalley scattering rate \hat{u}_i^1 and the intra-valley rate \hat{u}_z^1 , as

$$\hat{u}_i^1 = 4 \hat{u}_0^1 + 2 \hat{u}_z^1; \quad \hat{u}_z^1 = 4 \hat{u}_0^1 + 2 \hat{u}_{zz}^1: \quad (7)$$

Also, the trigonal warping term \hat{h}_w in the Hamiltonian (1) breaks the $p \perp p$ symmetry of the Fermi lines within each valley: $(K; p) \neq (K; p)$, while $(K; p) = (K; p)$ [9]. It has been noticed [17] that the deformation of a Fermi line of 2D electrons in GaAs/AlGaAs heterostructures in a strong in-plane magnetic field suppresses Cooperons as soon as the deformation violates $p \perp p$ symmetry. As \hat{h}_w has a similar effect, it enhances the relaxation rate of the pseudospin-triplet intervalley components C_0^x and C_0^y by

$$\hat{h}_w^1 = 2 \hat{u}_0^1 = \sim v^2: \quad (8)$$

However, since warping has an opposite effect on different valleys, it does not lead to relaxation of the pseudospin-singlet C_0^0 or the intervalley component of the pseudospin-triplet, C_0^z .

Altogether, the relaxation of modes C_0^1 can be described by the following combinations of rates:

$$\hat{u}_0^0 = 0; \quad \hat{u}_0^1 = 2 \hat{u}_i^1; \quad \hat{u}_0^2 = \hat{u}_0^1 = \hat{u}_w^1 + \hat{u}_z^1 + \hat{u}_i^1 = \hat{u}_0^1:$$

After we include dephasing due to an external magnetic field, $B = \text{rot}A$ and inelastic decoherence, γ^1 , the equations for C_0^1 read

$$D(\text{ir} + \frac{2e}{c\omega} A)^2 + \frac{1}{0} + \gamma^1 i! C_0^1(r; r^0) = \hat{u}(r^0):$$

(c). Due to the momentum-independent form of the current operator $\mathbf{v} = 2v\hat{u}$, the WL correction to conductivity g includes two additional diagrams, Fig. 1(e) and (f) besides the standard diagram shown in Fig. 1(d). Each of the diagrams in Fig. 1(e) and (f) [not included in the analysis in Ref. [12]] produces a contribution equal to $(\frac{1}{4})$ of that in Fig. 1(d). This partial cancellation, together with a factor of four from the vertex corrections and a factor of two from spin degeneracy leads to

$$g = \frac{2e^2 D}{\sim} \frac{d^2 q}{(2)^2} C_0^x + C_0^y + C_0^z = C_0^0: \quad (9)$$

Using expression Eq. (9), we find the $B = 0$ temperature dependent correction, $\gamma = g = g_0$, to the

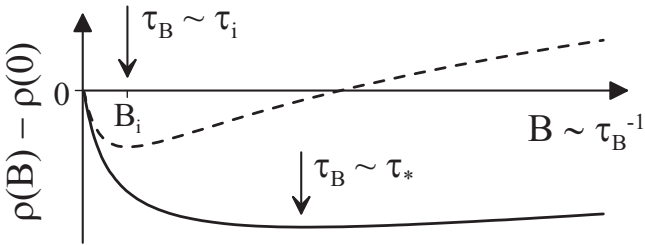


FIG. 2: Magnetoresistance expected in a phase-coherent (, \downarrow) graphene with $z; w$ (dashed) and i (solid line). In the latter case, arrows point at the field values where the rate of phase-breaking by a magnetic field is equal to the relaxation rates of relevant pseudospin-triplet Cooperon modes.

graphene sheet resistance. Taking into account the double spin degeneracy of carriers we present

$$\frac{\rho(0)}{2} = \frac{e^2}{h} \ln \left(1 + 2 \frac{B}{B_i} \right) - 2 \ln \frac{B}{1 + \frac{B}{B_i}} = \frac{tr}{\tau_i}; \quad (10)$$

and evaluate magnetoresistance, $\rho(B) = \rho(0) - \rho(B)$,

$$\rho(B) = \frac{e^2}{h} \left[F\left(\frac{B}{B_i}\right) - F\left(\frac{B}{B_i + 2B_i}\right) - 2F\left(\frac{B}{B_i + B}\right) \right]; \quad (11)$$

$$F(z) = \ln z + \left(\frac{1}{2} + \frac{1}{z} \right); B_{i,i} = \frac{\sim c}{4D e} \tau_i; \quad :$$

Here, $F(z)$ is the digamma function, and the decoherence (taken into account by the rate τ_i) determines the curvature of the magnetoresistance at $B = B_i$.

The last term in Eq. (9), C_0^0 is the only true gapless Cooperon mode which determines the dominance of the W L sign in the quantum correction to the conductivity in graphene with a long phase coherence time, $\tau_i > \tau_{tr}$. The two curves sketched in Fig. 2 illustrate the corresponding MR in two limits: $B = B_i$ ($z; w$ and i) and $B = B_i$ (i). In both cases, the low-field MR ($B = B_i$) is negative. If $B = B_i$, the MR changes sign: $\rho(B) < 0$

at $B = B_i$ ($\sim c = 4D e \tau_i$) and $\rho(B) > 0$ at higher fields. For $B > B_i$, the MR is distinctly of a W L type, with almost no sign of W AL. Note that in the latter case the W L magnetoresistance is saturated at $B = B_i$, in contrast to the W L MR in conventional electron systems, where the logarithmic field dependence extends into the field range of $\sim c = 4D e \tau_{tr}$. Such behavior is expected in graphene tightly coupled to the insulating substrate (which generates atomically sharp scatterers).

In a sheet loosely attached to a substrate (or suspended), the intervalley scattering time may be longer than the decoherence time, $\tau_i > \tau_{tr}$ ($B_i < B < B_i$). Hence C_0^z is effectively gapless, whereas trigonal warping suppresses the modes C_0^x and C_0^y . In this case the contribution from C_0^z cancels C_0^0 , and the MR would display neither W L nor W AL behavior: $\rho(B) = 0$.

Finally, in a narrow wire, with the transverse diffusion time $L^2/D = \tau_i$, the sample edges scatter between valleys [18]. Thus, when solving Cooperon equations in a wire, we estimate $\frac{1}{2} L^2 D = L^2$ for the pseudospin triplet, whereas the singlet C_0^0 remains gapless. This yields negative MR persistent over the field range $B > 2B_i$, where $B_i = \sim c = eL^2$:

$$\frac{\rho_{\text{wire}}(B)}{2} = \frac{2e^2 L}{h} \left[4 \frac{1}{1 + \frac{1}{3} B^2/B_i^2} \right] - 15; \quad (12)$$

The results of Eqs. (10-12) give a complete description of the W L effect in graphene and describe how the W L magnetoresistance reflects the degree of valley symmetry breaking in it. Eqs. (10-12) also show that, despite the chiral nature of electrons in graphene suggestive of antilocalisation, their long-range propagation in a real disordered material or a narrow wire cannot manifest the chirality. This observation explains the recent experiments [19, 20, 21] in which the low-field MR of a disordered graphene sheet displayed a distinctively weak localisation behavior.

We thank I. Aleiner, V. Cheianov, A. Geim, P. Kim, C. Marcus and K. Novoselov for discussions. This project has been funded by the EPSRC grant EP/C 511743.

[1] Y. Zheng, T. Ando, Phys. Rev. B 65, 245420 (2002); V. Gusynin, S. Sharapov, Phys. Rev. Lett. 95, 146801 (2005); A. Castro Neto, F. Guinea, N. Peres, Phys. Rev. B 73, 205408 (2006)

[2] D. Diienzo, E. Melé, Phys. Rev. B 29, 1685 (1984)

[3] T. Ando, T. Nakanishi, R. Saito, J. Phys. Soc. Japan 67, 2857 (1998)

[4] E. M. McCann and V. I. Fal'ko, Phys. Rev. Lett. 96, 086805 (2006)

[5] V. Cheianov and V. I. Fal'ko, cond-mat/0603624

[6] K. S. Novoselov et al., Nature 438, 197 (2005); K. Novoselov et al., Nature Physics 2, 177 (2006)

[7] Y. Zhang et al., Phys. Rev. Lett. 94, 176803 (2005); Y. Zhang et al., Nature 438, 201 (2005)

[8] T. Ando, J. Phys. Soc. Jpn. 74, 777 (2005)

[9] Here, we use notations in Ref. [4]. Comers of the hexagonal Brillouin zone are $K = (\frac{2\pi}{a}, 0)$, a being the lattice constant. The reversal of an operator \hat{W} is described by $(x, y) \hat{W} (x, y)$.

[10] B. L. Altshuler, D. K.hm el'itski, A. I. Larkin, P. A. Lee, Phys. Rev. B 22, 5142 (1980)

[11] S. Hikami, A. I. Larkin, N. Nagaosa, Progr. Theor. Phys. 63, 707 (1980)

[12] H. Suzuura, T. Ando, Phys. Rev. Lett. 89, 266603 (2002)

- [13] D .K hveshchenko, cond-mat/0602398
- [14] The group U_4 can be described using 16 generators
 $\hat{1}; s; 1; s_1, s; l = x; y; x.$
- [15] N .Shon, T .Ando, J. Phys. Soc. Jpn 67, 2421 (1998)
- [16] E .M cCann, V .Fal'ko, Phys. Rev. B 71, 085415 (2005);
 N .Peres, F .Guinea, A .Castro Neto, Phys. Rev. B 73, 125411 (2006); M .Foster, A .Ludwig, Phys. Rev. B 73, 155104 (2006)
- [17] V .Fal'ko, T .Jungwirth, Phys. Rev. B 65, 081306 (2002);
 D .Zumbuhle et al, Phys. Rev. B 69, 121305 (2004)
- [18] E .M cCann and V .I. Fal'ko, J. Phys. Cond. Matt. 16, 2371 (2004)
- [19] S.V .M orozov et al, cond-mat/0603826
- [20] C .M arcus, private communication
- [21] P K im , private communication